

Hybridization dynamics of surface immobilized DNA

Michael F. Hagan

Department of Chemical Engineering, University of California, Berkeley, California 94720

Arup K. Chakraborty^{a)}

Department of Chemical Engineering, Department of Chemistry, Biophysics Graduate Group, University of California, Berkeley, California 94720 and Physical Biosciences Division and Materials Science Division, Lawrence Berkeley National Laboratory, Berkeley, California 94720

(Received 5 November 2003; accepted 10 December 2003)

We model the hybridization kinetics of surface attached DNA oligomers with solubilized targets. Using both master equation and rate equation formalisms, we show that, for surface coverages at which the surface immobilized molecules interact, barriers to penetration create a distribution of target molecule concentrations within the adsorbed layer. By approximately enumerating probe and target conformations, we estimate the probability of overlap between complementary probe and target regions as a function of probe density and chain length. In agreement with experiments, we find that as probe molecules interact more strongly, fewer nucleation sites become accessible and binding rates are diminished relative to those in solution. Nucleation sites near the grafted end of the probes are least accessible; thus targets which preferentially bind to this region show more drastic rate reductions than those that bind near the free end of the probe. The implications of these results for DNA-based biosensors are discussed. © 2004 American Institute of Physics.

[DOI: 10.1063/1.1645786]

I. INTRODUCTION

Microdevices that detect the hybridization of surface attached DNA oligomers with solubilized target molecules are widely used in genomics applications, e.g., Ref. 1. Optical, electrochemical, and mechanical techniques have been used to develop devices that can not only discriminate between complementary and noncomplementary targets, but can even identify mismatches or length differences of a single nucleotide, e.g., Refs. 2–8. Designing or improving microdevices based on these methods requires an understanding of the kinetics of hybridization. Recent experiments reveal that the surface immobilization of “probe” oligomers can lead to hybridization kinetics that are significantly altered from those found in bulk solution. In particular, the observed rates depend on factors such as probe density,^{9–11} probe length,¹² location of the complementary sequence on the probe,^{13,14} and rates of diffusion from bulk solution.^{10,15} The coupled nature of these influences, however, makes experimental results difficult to interpret and sometimes even contradictory.

Chan *et al.*¹⁶ and more recently Erickson *et al.*¹⁷ have presented models that describe rates of surface hybridization in the limit of widely spaced, noninteracting probes. They find that adsorption of targets onto the surface reduces the dimensionality of diffusion and thereby enhances the overall flux of targets to reactive sites, leading to higher reaction rates. They find, in agreement with experiment,¹¹ that surface adsorption and thus reaction rates decrease as probe density is increased. Although it is possible to restrict probe densities to low levels for some immobilization methods,⁹ high probe

density may be desired to enhance signals in some devices.¹⁸ Thus, it is also important to understand hybridization kinetics at higher probe densities. Experiments show an extremely rapid decrease in observed rates as the overlap point is approached¹⁰ and exceeded.⁹

Studies of DNA hybridization in solution suggest that nucleation rates depend on two factors—the probability that complementary segments overlap and the rate of forming a nucleus once this overlap occurs.^{19,20} By limiting the access of target molecules to nucleation sites and impeding nucleation once overlap occurs, steric hindrances in a dense probe layer could affect both of these factors. It is difficult to separate these effects experimentally, since both factors presumably increase with increasing probe density, but in an unknown fashion. Two sets of experiments, however, suggest that limited access to nucleation sites may be the dominant factor. Peterson *et al.*^{13,14} measured rates of binding between a layer of 25-nucleotide probe molecules and two types of 18-nucleotide targets, one complementary to the upper portion of the probe (18 high) and the other complementary to the lower portion (18 low). Although these probe-target pairs have essentially identical binding kinetics in solution, Peterson *et al.* observed substantially slower binding to surface attached probes for the 18 low target as compared to the 18 high target (see Fig. 1). The authors point out that access to nucleation sites is diminished for the 18 low target because it has to penetrate into the probe layer to find complementary probe segments. Towery *et al.*²¹ measured hybridization rates for self-complementary sheared, genomic *E. Coli* DNA probes and targets. The reaction was carried out in a thin film of target solution that spanned only as high as the probe layer. Since the targets are entirely within the probe layer in

^{a)}Electronic mail: arup@uclink.berkeley.edu

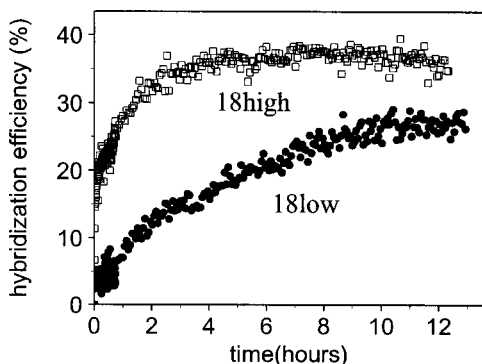


FIG. 1. Comparison of hybridization kinetics for targets complementary to the top (18 high) and bottom (18 low) of the probe (data originally shown in Fig. 1 of Ref. 13 and Fig. 1 of Ref. 14). The salt concentration is $C_s = 1$ M, and the probe density is $\sigma = 0.1$ chain/nm².

this experiment, penetration into the layer to find nucleation sites should not influence rates. The observed rates are, in fact, statistically identical to those measured for solution hybridization.

Schuck developed a model with which he showed that target diffusion often limits observed rates in a related system, where probes are immobilized within a thick (100–200 nm) hydrogel layer.^{22,23} The layer we consider, however, is only as big as the probe molecules from which it is composed, about 5–15 nm in typical experiments, and thus requires a different method of analysis. In this paper, we present a model with which we investigate how the structure of this layer inhibits transport of targets into the layer and subsequent coordination between complementary regions. We do not find that diffusion of targets is rate limiting in these systems. Instead, probe–probe and probe–target interactions create, even at equilibrium, an inhomogeneous distribution of probe and target nucleations sites, which decreases the number of available nucleation sites. We find that this effect can reduce effective hybridization rates by more than an order of magnitude, even if the intrinsic rates are unchanged from those in solution. The shielding of nucleation sites becomes more significant as probe interactions increase, either through higher surface coverage or longer chains. In addition, we show that predictions of the model are consistent with results from both of the experiments described above.

II. THEORY

Prediction of observed rates: We first present an overview of how kinetics are typically analyzed for hybridization on surfaces. We assume that diffusion from bulk is not a limiting factor, in order to focus on effects of probe–target distributions within the probe layer. The rate of production of hybridized molecules on the surface is usually analyzed according to Langmuir kinetics²⁴

$$\frac{dC_{PT}}{dt} = k_a C_B (\sigma - C_{PT}) - k_d C_{PT}, \quad (1)$$

where k_a and k_d are the association and dissociation rate constants, C_B is the bulk concentration of target molecules, C_{PT} is the surface concentration of hybridized molecules (in chains/area), and σ is the surface density of hybridized molecules at full coverage (equal to the probe density). If targets are in excess or continually replenished, this can be integrated to

$$C_{PT}(t) = C_{PT}^{eq} (1 - \exp(-k_s t)), \quad (2)$$

where $k_s = k_a C_B + k_d$ is the effective rate constant and the equilibrium density of hybridized chains is given by

$$C_{PT}^{eq} = \frac{k_a C_B \sigma}{k_s}. \quad (3)$$

Rate constants can be estimated by fitting experimental data to Eq. (3). The values obtained this way, however, are equivalent to the intrinsic rate constants only if C_B and σ reflect the distribution of target and probe nucleation sites throughout the probe layer. In this section, we examine how a depletion of target molecules in the layer and an inhomogeneous distribution of probe segments modify the observed rate constants.

We consider a layer of probes with N_P statistical segments of length l . (We use Tinland’s estimate of $l \approx 2$ nm for single stranded DNA,²⁵ or about five nucleotides.) We examine probe densities above the overlap threshold, $\sigma N_P l^2 \geq 1$, and thus make a mean field approximation in directions parallel to the surface. The perpendicular distance from the surface is denoted as z . Probe conformations are then determined by the distance of each segment, n , from the surface, given by $z(n)$.

To properly characterize the probe layer, we must specify probe and target concentrations within the layer in Eq. (3). A material balance shows that, for any segment n ,

$$\sigma = \int_0^h dz \frac{\phi_n(z)}{V_s}, \quad (4)$$

where h is the height of the layer, $\phi_n(z)$ is the volume fraction of n th segments at z , and V_s is the volume of a segment. Equation (1) can then be rewritten as

$$\frac{dC_{PT}}{dt} = k_a \int_0^h dz \left\{ C_B \frac{\phi_n(z)}{V_s} \left(1 - \frac{C_{PT}}{\sigma} \right) \right\} - k_d C_{PT}. \quad (5)$$

Now we modify Eq. (5) to allow inhomogeneous probe and target concentrations

$$\frac{dC_{PT}}{dt} = k_a \int_0^h dz \left\{ C_T(z) \Phi(z) \left(f_{\max} - \frac{C_{PT}}{\sigma} \right) \right\} - k_d C_{PT}, \quad (6)$$

where $C_T(z)$ denotes the concentration of target molecules with their forward most segment at position z and $\Phi(z)$ is the average of complementary probe concentrations over each target segment position,

$$\Phi(z) = \frac{1}{N_T} \sum_{n=1}^{N_T} \frac{\phi'_n[z(n)]}{V_s}, \quad (7)$$

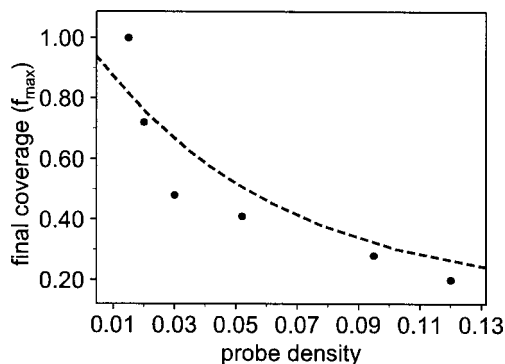


FIG. 2. Comparison of the fraction of probes available for hybridization (f_{\max}) predicted by the random adsorption simulation described in the text (dotted line) and the largest hybridization efficiencies recorded in Ref. 9 (points) (data from Fig. 4 of Ref. 26).

where N_T is the number of statistical segments in the target molecule and $\phi'_n[z(n)]$ denotes the concentration of probe segments that are complementary to segment n at the position $z(n)$. Since segments are composed of five nucleotides, there is at most one complementary segment per probe molecule for each target segment (for correctly selected sequences).

The maximum hybridization efficiency is now given by $f_{\max} \leq 1$ because a fraction of probes $(1 - f_{\max})$ are too close to neighbors for a target to bind at any time. Strey *et al.*^{27,28} showed that arrays of double stranded DNA molecules have strong repulsions between neighbors as the intermolecular distance is reduced below 3.2 nm, even at high salt concentrations. Thus, we might expect that once a target binds to a probe, binding is inhibited for any other probes within 3.2 nm. We calculated this quantity as a function of the probe density with Monte Carlo simulations, in which disks of radius 1 nm (equal to the radius of single stranded DNA) were randomly placed on the surface without overlapping. We then counted the maximum number of chains that could bind without having two hybridized molecules within 3.2 nm. This is clearly a crude approximation, especially at low probe densities, where close neighbors can avoid each other by tilting without approaching another molecule. Nevertheless, the resulting estimation of f_{\max} is in rough agreement with maximum hybridization efficiencies observed in experiments⁹ as a function of grafting density (see Fig. 2).

Comparison of Eq. (6) with Eq. (1) indicates that the observed rate constant is related to the intrinsic value as

$$\frac{k_{\text{eff}}}{k_a} = \frac{\int_0^h dz C_T(z) \Phi(z) f_{\max}}{C_B \sigma} \quad (8)$$

Since intrinsic rates are unknown, it is most instructive to compare the predicted surface hybridization rates with those observed in bulk solution. Observed rate constants in solution, k_a^B , are characterized by the Wetmur–Davidson relation,^{19,29} $k_a^B \sim L^2 k_N$ (for DNA concentrations in units of moles of chains/liter³⁰), where $L = 5N_T$ is the length of the DNA molecule. The elementary rate constant, k_N depends on the molecular weight as $k_N \sim L^{-0.5}$. The inverse dependence is attributed to the reduction of available nucleation sites due to excluded volume effects.^{19,20} Since the right-hand side of Eq. (8) determines the number of available nucleation sites in the probe layer, the predicted ratio of observed surface rate constants to those measured in bulk is given by

$$\frac{k_{\text{eff}}}{k_a^B L^{0.5}} = \frac{\int_0^h dz C_T(z) \Phi(z) f_{\max}}{C_B \sigma} \quad (9)$$

Since the layer structure and interactions in the layer will change as hybridization takes place, $C_T(z)$ and $\Phi(z)$ are time dependent quantities. In this work, we present calculations for these quantities based on the initial brush structure and thus determine only initial observed rates. The ramifications of the changing brush structure are considered qualitatively in Sec. V.

Because we determine that diffusion of target molecules within the brush is not a limiting factor (see Sec. IV A), target concentrations within the layer satisfy the Boltzmann distribution $C_T(z) = C_B \exp[-w(z)]$, where $w(z)$ is the potential, in units of the thermal energy ($k_B T$), to insert a target into the layer at position z . We present calculations for both $w(z)$ and $\Phi(z)$ in the Appendix, based on the Misra *et al.* polyelectrolyte brush theory³¹ and Milner's calculation of the potential to insert a chain into a neutral brush.³²

III. FORMULATION OF THE MASTER EQUATION

We have heretofore assumed that rates of probe–target nucleation are slow compared to transport into the brush and post-nucleation zipping of base pairs. We can relax these assumptions by characterizing the time evolution of the system with a master equation formalism. We denote the time dependent probability that the lead segment of a target chain is in layer z with m statistical segments bound as $P(z, m, t)$. The rate of change of probability is then³³

$$\begin{aligned} \frac{dP(z, m, t)}{dt} = & \omega_{z, z+1}(z+1, m)P(z+1, m, t) + \omega_{z, z-1}(z-1, m)P(z-1, m, t) \\ & - (\omega_{z+1, z}(z, m) + \omega_{z-1, z}(z, m))P(z, m, t) + \bar{\omega}_{m, m+1}(z, m+1)P(z, m+1, t) + \bar{\omega}_{m, m-1}(z, m-1)P(z, m-1, t) \\ & - (\bar{\omega}_{m+1, m}(z, m) + \bar{\omega}_{m-1, m}(z, m))P(z, m, t), \end{aligned} \quad (10)$$

where $\omega_{z,z'}$ and $\bar{\omega}_{m,m'}$ are transition rates for hopping between layers and binding or unbinding of segments, respectively. Hopping rates are chosen to satisfy detailed balance³³

$$\omega_{z',z} = \delta_{m,0} \frac{D\left(\frac{z+z'}{2}\right)}{\Delta^2} \exp\left[w(z) - w\left(\frac{z+z'}{2}\right)\right], \quad (11)$$

where the Kronecker delta function enforces that hopping is only possible if no segments are bound and Δ is the distance between layers. The diffusion coefficient, $D(z)$, is determined within a Zimm model,³⁴ as suggested by Milner:³² the penetrating target forms a string of “blobs” of size ξ and the friction factor is given by the Stokes formula summed over each blob $\sum_i 6\pi\eta\xi_i = 6\pi\eta(h-z)$, where η is the viscosity. The diffusion coefficient is then given by the Einstein formula

$$D(z) = \frac{k_B T}{6\pi\eta \max[(h-z), R_h]}, \quad (12)$$

where the max function in the denominator ensures that this formula reduces to the bulk diffusion coefficient as the chain leaves the brush. The hydraulic radius is given by $R_h = R_g/2$ (Ref. 25) and the radius of gyration is given by $R_g^2 = N_T l^2/6$. Since the brush is solvated, we use $\eta = 1.5$ cp.

The variable m describes binding of statistical segments (about five nucleotides²⁵). As this is close to the number of base pairs required for nucleation,^{35–37} the rate of binding for the first segment is equal to the nucleation rate

$$\bar{\omega}_{1,0}(z,0) = k_a \Phi(z) \left(f_{\max} - \frac{C_{PT}}{\sigma} \right). \quad (13)$$

After enough base pairs have bound to form a stable nucleus, it is generally assumed that the remaining bases bind in a rapid zipping motion. Zipping is a first order reaction, with a forward rate for the binding of one base-pair of $k_1 \approx 10^7 \text{ s}^{-1}$, while the reverse rates, k_{-1} are 5–10 times slower.^{35–37} Because we consider binding at the statistical segment level, we solve for the rate of five bases binding by determining the first passage time for an asymmetric random walk with a reflecting boundary at $m=0$ bases bound and an absorbing boundary at $m=5$ bound.³⁸ The forward and reverse transition rates given by the base-pair binding and unbinding rates (k_1 and k_{-1}), which gives

$$k_f^{-1} = \frac{n_s}{k_1 - k_{-1}} + \frac{k_{-1}}{(k_1 - k_{-1})^2} \left(\frac{k_{-1}}{k_1} \right)^{n_s}, \quad (14)$$

where $n_s = 5$ is the number of bases in a statistical segment. The segment dissociation rate is then obtained by interchanging k_1 and k_{-1} .

We now consider the effect of interactions within the probe layer on the zipping process. As in the development of the rate equation (Sec. II A), we assume that the target can enter with a forward (0th segment first) or reverse (N th segment first) orientation. In the case of forward entry, the probe segments that are complementary to the leading target segments are confined near the surface. Thus, the target has to penetrate almost to the surface before the nucleation rate becomes nonzero. At this point the chain is already mostly

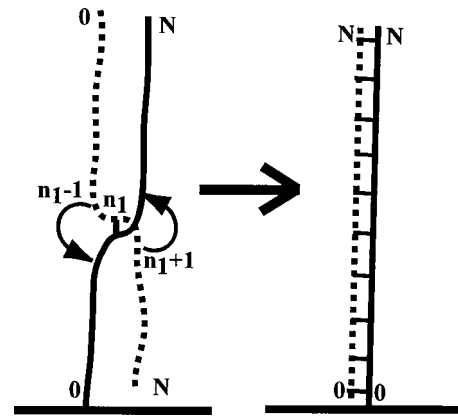


FIG. 3. Model for zipping of a reverse entry target. The target (solid line) binds with segment n_1 . Subsequent binding can occur when segment $n_1 + 1$ diffuses up to the next position on the probe (dotted line) or when $n_1 - 1$ diffuses down to the next position. The process ends with the target in the same orientation as the probe, as shown on the right-hand side.

aligned with its binding partner, so no large-scale motions are required, and we assume zipping proceeds as in solution.

In the case of reverse entry, finite nucleation rates exist throughout the brush, but the zipping process involves target motions on the scale of the brush height. For example, if nucleation occurs near the edge of the brush ($z \approx h$), the entire target must penetrate into the brush during zipping. The mean first passage time for an unbound target to penetrate to the surface can be calculated from Eqs. (10) and (11) (Refs. 33 and 39) and is long compared to nucleation times. Even so, the following model suggests that the zipping process still proceeds much faster than nucleation rates.

We consider a target chain for which the N th segment is at z and segment n_1 is bound to a probe chain (see Fig. 3). We treat the target as two chains that can move independently, but are both tethered to the probe at segment n_1 . For segment $n_1 - 1$ to bind, the upper portion of the chain ($n < n_1$) must penetrate into the brush until segment $n_1 - 1$ moves one position below segment n_1 , where its complement is found on the probe chain. Likewise, segment $n_1 + 1$ can only bind if the lower portion of the chain diffuses backward until overlap occurs one position up from $z(n_1)$. Upon completion of zipping, the target has executed a flip-flop—the upper partial chain is bound below segment n_1 and the lower portion has moved up. We describe the motion of the partial chains in the same manner as the penetration of the entire target, except the potential $w[z(n_1 - 1)]$ and the diffusion constant are determined for a chain of length $N = n_1 - 1$. The partial chain length decreases as more segments bind.

The upper partial chain is diffusing against a potential gradient and, as mentioned above, the time scale for completion of this process without binding is long. The fact that the forward binding rate is much greater than the segment dissociation rate, however, redefines the nature of the motion. The chain has to diffuse a distance $\sim l$ before a binding event can take place. We show below that the time required to diffuse over this distance is comparable to forward binding rates. Once binding occurs, the partial chain is tethered one

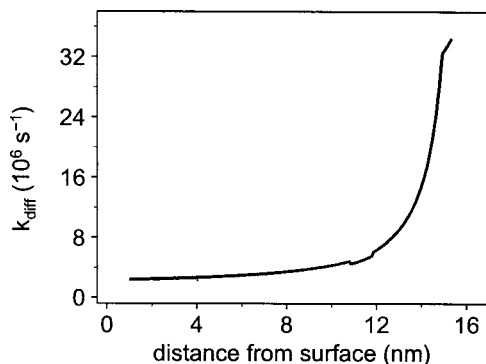


FIG. 4. Calculated rates for diffusion, k_{diff} , of partial chain into position for segment zipping for a reverse oriented target. Parameters are $\sigma=0.1$, $N_T=N_p=10$, and $C_S=1$ M. Binding is assumed to occur at the middle of the brush, thus the initial partial chain length is $N_p/2$. For simplicity, this value is assumed constant throughout the zipping process.

segment further down the probe and thus cannot diffuse back unless a relatively improbable dissociation event occurs. In this way, the process of zipping acts like a Brownian ratchet.^{40,41} Since the intersegment diffusion rates are comparable to the binding rates, the overall zipping rate is similar to that found in solution.

IV. RESULTS

A. Comparison of diffusion and binding rates

Passage from the master equation formalism of Sec. III to the rate equation used in Sec. II is only valid if nucleation rates are much slower than both target transport and zipping rates. We first verify that zipping within the brush is fast compared to nucleation rates (see Sec. III). For a statistical segment length of five nucleotides and nucleotide binding rates³⁶ of $k_1=10^7 \text{ s}^{-1}$ and $k_{-1}=2 \times 10^6 \text{ s}^{-1}$, Eq. (14) gives a segment binding rate of $k_f=1.6 \times 10^6 \text{ s}^{-1}$ and a dissociation rate of $k_b=2 \times 10^3 \text{ s}^{-1}$. As described in Sec. III, a partial chain must diffuse a distance $\sim l$ before the next forward binding event can take place. The first passage time for this process is calculated using Eq. (11) with $\Delta=l$. The resulting diffusive rates for a typical system are shown in Fig. 4.

This calculation under predicted the rates by choosing the maximum possible partial chain length at all stages of zipping, but the resulting rates are still larger than the association rate constant. The net rate for a segment to bind can be approximated as $k_{f,\text{eff}}^{-1} \approx (k_{\text{diff}} + k_f)^{-1}$ and is orders of magnitude larger than the reverse rate. Thus, an unbinding event is extremely improbable in the time required to bind an additional segment and zipping proceeds according to the ratchet mechanism discussed in Sec. III, with a similar rate to that in bulk solution.

The assumption that nucleation, rather than target transport, is rate limiting can be validated by calculating a Damköhler number (D_a),⁴³ given by the ratio of characteristic reaction and diffusion rates

$$D_a(z) = \frac{\text{reactive flux}}{\text{diffusive flux}} = \frac{k_a C_T(z) \int_0^h \Phi(z) dz}{C_T(z) \left(D(z) \frac{dw(z)}{dz} \right) \Big|_{z=0}}, \quad (15)$$

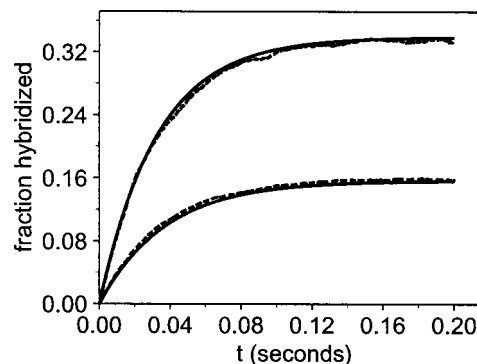


FIG. 5. Comparison of hybridization efficiencies predicted by the rate equation, Eq. (8) (solid lines), and the master equation, Eq. (10) (dashed lines). To decrease the computation time, the target concentration ($C_B=10^{-3}$ M) is three orders of magnitude higher than those used in typical experiments. This does not affect the Damköhler number, Eq. (15). The master equation was simulated using the Gillespie algorithm (Ref. 42). Parameters are $k_a=10^6 \text{ M}^{-1} \text{ s}^{-1}$, $k_d=5 \text{ s}^{-1}$, $N_p=N_T=7$ segments. For the upper curve $\sigma=0.07$ chain/nm² and $C_S=0.5$ M, while for the lower curve $\sigma=0.15$ chain/nm² and $C_S=1$ M.

where the denominator follows from Eq. (8) in Milner's work.³² Small values of the Damköhler number indicate that the system is reaction-rate limited. We find that $D_a(z) \lesssim 10^{-2}$ for all cases we consider. This suggests that the rate equation is a good approximation for Eq. (10). A comparison of results from the two formalisms confirms this prediction; results for a typical case are shown in Fig. 5.

B. Predicted effective nucleation rates, k_{eff}

In this section we examine the variation of the observed rates as predicted by Eq. (8) and, to the extent that is possible, compare the results with experimental data. For simplicity, we keep $N_T=N_p$, except where otherwise noted.

The variation of k_{eff}/k_a^B with probe density for several chain lengths is shown in Fig. 6. It is not surprising that the observed rate constant decreases with increasing probe density, as additional probes increase both steric hindrance effects and electrostatic repulsions. This is manifested in Eq. (8) in two ways: a higher target insertion potential, $w(z)$, which results in a lower effective target concentration, $C_T(z)$ and a smaller number of viable probes (f_{max}). A log-log scale is used to emphasize the fact that for long enough

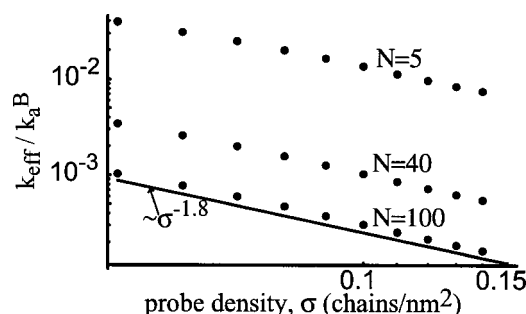


FIG. 6. Variation of effective association rate constant (normalized by bulk rate constant) calculated with Eq. (9). Salt concentration is $C_S=1$ M and $N_p=N_T=5, 40$, and 100 for the upper, middle, and lower curves, respectively. The line is drawn to demonstrate scaling of $\sigma^{-1.8}$.

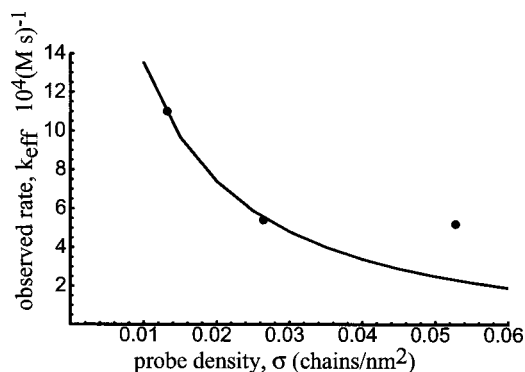


FIG. 7. Comparison of predicted initial rate constants (line) and those observed in Henry *et al.* (Ref. 10) (points). The bulk solution value measured in Ref. 10 is $5 \times 10^5 \text{ M}^{-1} \text{ s}^{-1}$ and the salt concentration is $C_S = 0.1 \text{ M}$ (Ref. 44). The chain lengths were $N_p = N_T = 5$, which corresponds to 25 nucleotides. The experiments used 22-nucleotide molecules.

chains ($N \geq 20$) and large enough probe densities ($\sigma \geq 0.05 \text{ chains/nm}^2$) the effective rates scale approximately as $k_{\text{eff}} \sim \sigma^{-1.8}$.

Although a decrease in observed rate constants with increasing probe densities has been seen in several experiments,^{9–11} comparison of the predicted trend to experimental data is complicated in many cases by effects of target transport from bulk to the surface.⁴³ Henry *et al.*¹⁰ ensure that diffusion from bulk does not limit rates by attaching probes to microparticles, which minimizes the size of the diffusion boundary layer. Since these microparticles are large (radius $\sim \mu\text{m}$) compared to the size of the DNA, it is not necessary to consider effects of curvature in our calculation. The predicted ratio k_{eff} is compared to their initial rates in Fig. 7, where the value $k_a^B = 5 \times 10^5 \text{ M}^{-1} \text{ s}^{-1}$ used in the model is taken from the association rate constant measured in bulk solution. The agreement is (perhaps fortuitously) quite good, considering that there are no fit parameters and the probe densities are relatively low.

Georgiadis and co-workers⁹ used surface plasmon resonance (SPR) to measure hybridization efficiencies as a function of time for various probe densities. The probes are attached to a planar surface in this case; therefore, it is likely that rates are influenced by diffusion from bulk to the surface.¹⁵ This is further suggested by the fact that the initial rate constants we obtain from their data are an order of magnitude smaller than those recorded in Henry *et al.*¹⁰ (compare Fig. 8 to Fig. 7). However, the data is not consistent with a model in which diffusion to the surface is the sole limiting step because the overall rates of hybridization (not normalized by the probe density) decrease with increasing probe density. If diffusion to the surface were rate limiting, the initial values of these rates would be related to flux across a boundary layer and independent of probe density. Furthermore, experiments carried out on the same apparatus discussed in the next paragraph clearly demonstrate that the structure of the probe layer affects rates. Therefore, we compare effective rate constants predicted from our model to the experimental values. Effects of diffusion from bulk are incorporated in the simplest way possible—we assume that the target concentration at the edge of the brush is diminished

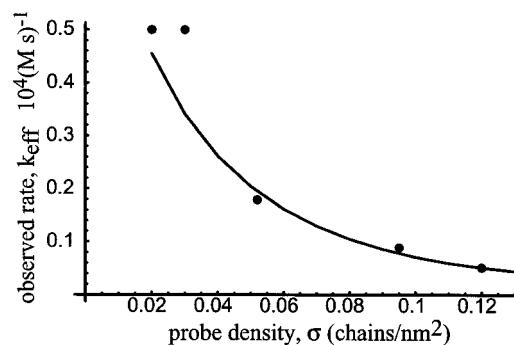


FIG. 8. Comparison of predicted initial rate constants (line) and values fit from data in Fig. 4 of Ref. 9 (black points). The theoretical values are scaled by the experimental value at $\sigma = 0.12 \text{ chains/nm}^2$ because there is no measured solution rate constant. Salt concentration is $C_S = 1 \text{ M}$ and $N_p = N_T = 5$, to correspond to the 25-nucleotide molecules used in the experiments.

compared to the bulk value (C_B) and thus the concentrations in the brush are reduced by a multiplicative factor. As we do not have a measured solution rate constant for this molecule anyway, we use one data point ($\sigma = 0.12 \text{ chains/nm}^2$) to fit both an intrinsic rate constant and the concentration factor, which enter Eq. (8) as one parameter. With just this parameter, we find that the predicted effective rates for the other probe densities are similar to the experimental values (see Fig. 8).

Georgiadis and co-workers have also used SPR to make a more unexpected observation—targets that are the same length and bind to surfaces with the same probe density can still exhibit different binding rates if they are complementary to different regions on the probe^{13,14} (see Sec. I and Fig. 1). If this difference results from steric effects of the probes, as the authors suggest, our model should also predict different rates for these targets. Since the model can only recognize complementarity on the scale of a statistical segment, we compare effective initial rates for target chains of $N_T = 3$ segments (15 nucleotides) that bind to the top or bottom of probes that are $N_p = 5$ segments in length (25 nucleotides). At the experimental probe density (0.03 chains/nm^2), the predicted ratio of binding rates (18 low/18 high) for the two targets is equal to the ratio we obtain from the experimental data, 0.3. If we use $N_T = 4$ (20 nucleotides) we obtain a somewhat higher ratio of 0.5.

Based on either of these predicted values, it is clear that the model at least qualitatively captures the effect seen experimentally. At a lower probe density ($0.015 \text{ chains/nm}^2$), however, the experimental rates for the two targets are almost indistinguishable, while the model predicts ratios that are only slightly higher than those at 0.03 chains/nm^2 . This discrepancy may be a reminder that we assumed probe densities were above the overlap threshold ($\sigma \sim 0.11 \text{ chains/nm}^2$ for $N_p = 5$) when developing the model. Above this point, the predicted dependence of observed rates on complementary location increases dramatically as either the length of the nonoverlapping region or the probe density increases (see Fig. 9).

Interactions between probes become more significant not only as more probes are added, but also as the probe length increases. Consequently, model predictions show a decrease

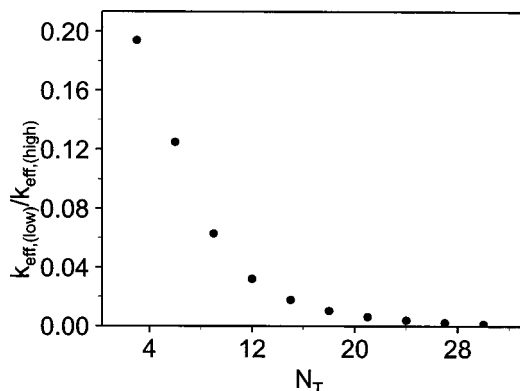


FIG. 9. Predicted ratio of initial rates for targets complementary to upper and lower portions of probe. In all cases, the ratio of $N_T/N_p=3/5$, $C_S=1$ M, and $\sigma=0.1$ chain/nm².

in the effective rate constant with chain length (see Fig. 10). The same approximate scaling is seen for all probe densities and salt concentrations, $k_{\text{eff}}/k_a^B \sim N_T^{-0.8}$. This scaling can be qualitatively understood as follows. Target chains typically only penetrate to a point at which $w(z) \sim k_B T$. This penetration depth increases slightly with probe length, but the probe layer height increases as $h \sim N_p$. Thus, the accessible fraction of the probe layer, and therefore the fraction of available nucleation sites, decreases nearly inversely with chain length.

The variation of surface hybridization rates with chain length has been explored in only one set of experiments. Okahata *et al.*¹² used a quartz crystal microbalance to measure kinetics of hybridization for target and probe complements of 10, 20, and 30 nucleotides. The observed initial rates (see Fig. 11) are surprising in that they increase with chain length even faster than the Wetmur–Davidson relation^{19,20} predicts for reactions in solution ($k_a^B \sim L^{1.5}$ for DNA concentrations given in units of moles chains/liter³⁰). Our theory, on the other hand, predicts a slower increase with chain length as compared to solution values. This comparison is shown in Fig. 11. Since our theory yields rate constants normalized by the bulk solution value, which is not measured for this case, the theoretical values in Fig. 11 were multiplied by a factor of $L^{1.5}$ and then normalized to be equal to the experimental value at 10 nucleotides. As explained

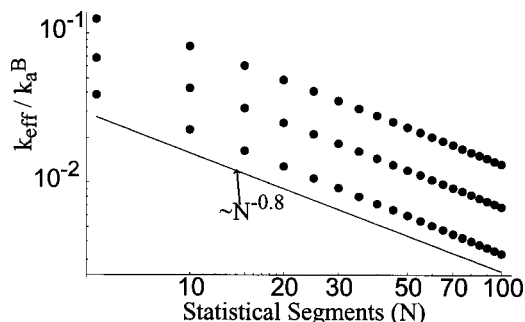


FIG. 10. Predicted variation of effective rate constant with chain length, normalized by bulk rate constant. The two upper curves are for $C_S=1$ M and $\sigma=0.07$ and 0.1 chains/nm², and the lower curve is for $C_S=0.4$ M and $\sigma=0.1$. The line demonstrates scaling of $N_T^{-0.8}$.

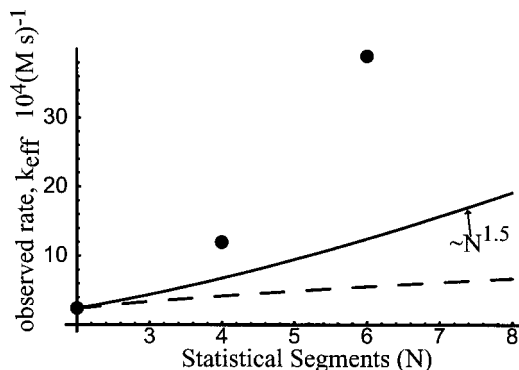


FIG. 11. Comparison of variation of rate constants with chain length predicted by theory (dashed line) and data in Okahata *et al.* (Ref. 12) (points). Because we do not know the solution rate constant, and Eq. (9) predicts rates relative to those in bulk solution, we multiplied the predicted values by the Wetmur–Davidson variation with chain length, $L^{1.5}$, and scaled to match the experimental data at 10 nucleotides ($N_T=2$ segments). The parameters are $\sigma=0.12$ chains/nm² and $C_S=0.2$ M (Ref. 44), $T=20$ °C. The line indicates the variation of rate constants in solution, as predicted by the Wetmur–Davidson relationship (Refs. 19 and 20) (also scaled to match experimental data at 10 nucleotides).

above, the result from our theory is consistent with intuition because the fraction of accessible nucleation sites in the probe layer should decrease with chain length faster than in solution.

The rapid increase in experimental rates can in part be explained by the fact that the melting temperature, T_m , increases with chain length. The nucleation rate constant increases with $T_m - T$ up to a value of 25°. The value of $T_m - T$ for the 10-nucleotide chain in this experiment is only about 5°. This effect is not incorporated in the model predictions. We also note, however, that the model development assumes “long” chains. This requirement is clearly violated by a chain length of 10 nucleotides, which corresponds to only two segments.

We cannot completely determine the extent to which our model captures surface hybridization kinetics without more experimental data to compare with. The comparisons in this section, though, illustrate how important understanding these kinetics can be for microdevice design. In many cases, high probe densities are desired in order to increase signal strength and thus decrease detection limits. However, binding rates can become prohibitively slow at higher densities. Lower hybridization efficiency translates to a weaker recognition signal. Thus, there is an optimal probe density which can only be determined by considering both equilibrium and kinetic factors. Figures 1 and 9 highlight the fact that the optimal probe density decreases significantly if targets cannot bind to regions of the probes that are found at the periphery of the brush. This also suggests that mismatches between targets and probe regions near the grafting end should reduce binding rates less than those near the free end, as seen in recent experiments.⁸

V. OUTLOOK AND CONCLUSIONS

Although the comparisons we have made between initial rates predicted by our model and those seen in experiments are mostly favorable, one or more assumptions

were violated in some cases. We still made these comparisons because only a limited amount of data is available in this regime. Considering the importance of these rates to the rapidly growing field of device design, we hope that more experiments will be carried out in regions where the model applies. Many experiments and microdevices are designed for short chains, however, so it may also be desirable to modify the model so that it applies to shorter chains, as discussed in the Appendix.

The other significant limitation of the model is that we only predict initial rates, since we neglect the change in the structure of the probe layer upon hybridization. Hybridized DNA is effectively a rod at the lengths we consider⁴⁵ and thus the ends of all hybridized molecules will be located near the edge of the brush. In analogy to a brush composed of different length chains, the ends of the more flexible single stranded probes will then be found closer to the surface,⁴⁶ thereby reducing the concentration of available nucleation sites. In addition, arrays of double stranded DNA molecules are known to have strong repulsive lateral interactions.^{27,28} Thus, the potential felt by a penetrating target, $w(z)$, presumably increases as hybridization occurs. Incorporation of these effects may lead to biexponential hybridization rates, such as has been seen in experiments.¹⁰

We have also assumed that the intrinsic rate of nucleation for overlapping segments is the same in a brush as in bulk solution. The effect of the impenetrable surface and crowding due to neighboring probes on segment–segment binding rates can be explored with atomistic simulations; some atomistic investigations of DNA base-pair binding/unbinding have already been carried out.^{47–51} Our model provides an avenue by which the microscopic results of these simulations can be connected to macroscopic experimental observables, such as overall binding rates. Towery *et al.* observed, however, that rate constants for probe–target binding in thin films are the same as those in solution if the target solution is confined within the probe layer.²¹ When targets are thus confined, the target distribution, $C_T(z)$, is forced to be more or less homogeneous throughout the layer and all probe segments are equally accessible. Thus, in this situation, our model would predict that the measured rates should share the same relation to intrinsic rates as those measured in bulk. Therefore, the experimental findings suggest that intrinsic rates may not change within the probe layer.

Finally, we have neglected attractions between DNA and the surface in this model. Attractions were shown to have a significant effect on rates at low probe densities^{16,17} because adsorption onto the surface reduces the dimensionality of diffusion. While lateral diffusion on the surface is probably not a factor at high density, attractions could change the equilibrium distribution of targets, $C_T(z)$. This effect should diminish as the probe interactions increase, since the amount of adsorbed targets will depend on the ratio of the strengths of the attraction to the surface and the potential to insert a chain, $w(z)$.³²

We have presented a model with which we predict effective rates of DNA hybridization between solubilized targets and dense layers of surface attached probes. Together with analyses developed for low probe density,^{16,17} this model al-

lows the examination of rates over all relevant densities. We find that, at high probe densities, barriers to target penetration into the probe layer can reduce observed rate constants by an order of magnitude, as seen experimentally.^{9,10} We hope that this model can serve as a guide and motivation for future experiments. In particular, the variation of rates with chain length warrants further investigation.

ACKNOWLEDGMENTS

Financial support for this work was provided by the Defense Advanced Research Project Agency (DARPA). We acknowledge fruitful discussions with (and data from) Professor Rosina Georgiadis and Yang Gao. M.F.H. also thanks David Bindel for helpful discussions.

APPENDIX

In the following we calculate the quantities $C_T(z)$ and $\Phi(z)$ using the Misra *et al.* polyelectrolyte brush theory³¹ (hereafter referred to as Misra). This theory is an extension of the Milner *et al.* theory for a neutral polymer brush⁵² (hereafter referred to as MWC) and is technically valid only in the long chain limit. The experiments we consider, however, are usually confined to short chains (~ 5 – 10 segments), and thus a discrete theory such as the method of Scheutjens and Fleer⁵³ might be more appropriate. We use the Misra theory because it provides analytical results; our calculations can easily be adapted to another method.

Polymer brush theories

We begin by briefly reviewing the MWC and Misra theories. For grafting densities (σ) well above the overlap threshold, De Gennes⁵⁴ predicted that the height of the layer is proportional to the length of the grafted chains, $h \sim N_p$ and thus the chains are strongly stretched as compared to the radius of gyration of an unperturbed chain, $h \gg R_g \sim N_p^{1/2}$. The change in free energy upon inserting one chain into the brush, or the chemical potential of a chain, is given by

$$\mu = \int_0^{N_p} dn \left\{ \frac{1}{2l^2} \left(\frac{dz}{dn} \right)^2 + U[z(n)] \right\}. \quad (\text{A1})$$

The first term on the right-hand side accounts for the elasticity of the chain, and the second term, U , is the mean-field potential in the layer due to the grafted chains. All energies are given in units of the thermal energy ($k_B T$). As first shown by Semenov,⁵⁵ the condition of strong stretching restricts chain conformations to only small fluctuations about the most probable path, in analogy to the classical limit of quantum mechanics. Chain conformations then take the form of a classical particle moving in a potential

$$\frac{d^2 z}{dn^2} = - \frac{dU(z)}{dz}, \quad (\text{A2})$$

with the initial condition $z(0) = 0$, since all chains are grafted to the surface, and the condition

$$\left. \frac{dz(n)}{dn} \right|_p = 0, \quad (\text{A3})$$

which states that the tension vanishes at the end of the chain, $z = \rho$, because the chain is in mechanical equilibrium. Semenov and MWC show that the brush free energy is minimized if chain ends are dispersed throughout the brush. Since the chains are monodisperse, each chain must reach the surface in the same number of steps regardless of its end position, which restricts the potential to a parabolic form

$$-U(z) = A - Bz^2, \quad (\text{A4})$$

where $B = \pi^2/8N^2l^2$.⁵²

Misra *et al.*³¹ extend this theory to polyelectrolyte brushes by including electrostatic effects in the mean field, $-U(z) = -U_N(z) - U_E(z)$, where the nonelectrostatic interactions are given by

$$-U_N(z) = -\log(1 - \phi(z)) - 2\chi\phi, \quad (\text{A5})$$

where $\phi(z) = \int_0^{N_p} dn \phi_n(z)$ is the overall volume fraction, and the electrostatic energy is given by

$$-U_E(z) = V_p e \psi(z), \quad (\text{A6})$$

where V_p is the number of charges per segment, e is the charge of an proton, and ψ is the electrostatic potential. The authors simultaneously solve the Poisson-Boltzmann equation for $\psi(z)$ and Eq. (A4) for the volume fraction, $\phi(z)$. These equations have to be solved numerically.

In this work we assume that counterion condensation reduces the effective charge of DNA as described by Manning,⁵⁶⁻⁶⁰ thus $V_p = l/l_b$, where l_b is the Bjerrum length. We also assume that water is nearly a theta solvent for DNA²⁵ and take $\chi = 0.45$.

Calculation of $\Phi(z)$

We begin by determining the individual segment volume fractions for the probe molecules, $\phi_n(z)$. We solve Eq. (A2) to obtain the conformation of a chain ending at ρ

$$z(n; \rho) = \rho \sin\left(\frac{\pi n}{2N_p}\right). \quad (\text{A7})$$

The segment volume fraction is thus given by

$$\phi_n(z) = \phi_N \left(\frac{z}{\sin\left(\frac{\pi n}{2N_p}\right)} \right). \quad (\text{A8})$$

Semenov⁵⁵ and MWC observed that the endpoint distribution, $\phi_N(z)$, can be found from the inverse equation

$$\phi(z) = \int_z^h d\rho \phi_N(\rho) \frac{dn}{dz}(\rho; z), \quad (\text{A9})$$

where the tension is found from Eq. (A7),

$$\frac{dz}{dn}(\rho; z) = \frac{\pi(\rho^2 - z^2)^{1/2}}{2N_p}. \quad (\text{A10})$$

Since we solve the brush equations numerically, ϕ is only known at discrete intervals and Eq. (A9) becomes a matrix equation. The kernel is singular at $z = \rho$, so we linearly interpolate $\phi_N(z)$ between layers z_i ,

$$\hat{\phi}_N(x) = \phi_N(z_i) + \frac{\phi_N(z_{i+1}) - \phi_N(z_i)}{z_{i+1} - z_i} (x - z_i), \quad (\text{A11})$$

which results in

$$\phi = \underline{\underline{\Lambda}} \phi_N, \quad (\text{A12})$$

where the elements of ϕ and ϕ_N are the values of the volume fractions in each layer and $\underline{\underline{\Lambda}}$ is an upper triangular matrix. We solve for ϕ_N with backsubstitution.

We now determine the conformation of the target molecule. Milner³² suggests that the portion of the target inside the brush takes the conformation of the most stretched chain in the brush ($\rho = h$), while the portion outside the brush remains in a random coil conformation. For simplicity, we assume that half the chains enter with segment 0 first (forward entry), while the other half enter with segment N first (reverse entry). It is possible to relax this assumption and allow any segment to enter first, but the calculation is more complicated and yields similar results. Using Eq. (A7) we find that the position of segment n of a forward target with lead segment at z' (or segment $N - n$ of a target which entered in reverse) is given by

$$z(n, z') = h \left[\left(1 - \left(\frac{z'}{h} \right)^{1/2} \right) \sin\left(\frac{\pi n}{2N_p}\right) + \frac{z'}{h} \cos\left(\frac{\pi n}{2N_p}\right) \right] \text{ for } n \leq N_p - n_2, \quad (\text{A13})$$

where n_2 is the rank of the segment on the most stretched chain at position z' and is found from Eq. (A7).

If the target completely enters the brush, with an endpoint $h_T(z') \leq h$, Milner³² suggests that the chain takes the conformation of the probe chain with the same endpoint ($\rho = h_T$). In this case, $n_2 = N_p - N_T$ and we solve for the endpoint as

$$h_T(z) = \frac{z}{\sin\left(\frac{\pi(N_p - N_T)}{2N_p}\right)} \text{ for } z' \leq h \sin\left(\frac{\pi(N_p - N_T)}{2N_p}\right). \quad (\text{A14})$$

The position of each segment can be obtained with Eq. (A7).

The quantity $\Phi(z)$ is now calculated by converting Eq. (7) into an integral over z , where Eq. (A10) is the Jacobian, and $\phi_N(z)$ is interpolated as in Eq. (A11).

Calculation of $w(z)$

In this section we calculate $w(z)$, the potential of a target chain with lead segment at z , relative to a random coil in solution. In Ref. 32 Milner uses results from MWC to calculate this potential for a neutral chain with the same length as the grafted chains. He also presents arguments that suggest how to carry out this calculation in the case of a shorter target chain. In this section, we carry out both calculations, modified for use with the Misra theory.

Milner observes that the force to hold the lead segment of a chain at z is equal and opposite to the tension on this segment, $(dz/dn)(0; z)$. The total work to bring a chain to z from outside the brush is then given by

$$w_n(z) = \int_z^h dz' \frac{1}{l^2} \frac{dz}{dn}(0; z'), \quad (\text{A15})$$

where we label the potential as w_n to signify it is for a neutral brush. In the case of a polyelectrolyte brush, the mean-field potential, $U(z)$, does not vanish at the edge of the brush, but is equal to the electrostatic potential. Outside the brush, the potential decays exponentially in accordance with Guoy–Chapman theory.³¹ Thus, there is an extra term associated with the work to bring the chain across this tail region. Since we find that the decay length is small compared to the size of the chain in solution ($\sim N_T^{1/2}$), we assume that only the monomers inside the brush have overcome this potential. The chain insertion potential for a polyelectrolyte brush is therefore

$$w(z) = \int_z^h dz' \frac{1}{l^2} \frac{dz}{dn}(0; z') + U(h) \frac{h-z}{h} N_T. \quad (\text{A16})$$

Milner points out that the equation of motion governing chain conformations, Eq. (A2), implies a conservation of “energy,”

$$E = \frac{1}{2l^2} \left(\frac{dz}{dn} \right)^2 - U(z). \quad (\text{A17})$$

Since the tension must vanish at the edge of the brush or the endpoint of the target chain [$h_T(z) \leq h$], this gives the tension as

$$\frac{1}{l^2} \frac{dz}{dn} = (2B)^{1/2} \left(1 - \left(\frac{z}{h_T(z)} \right)^2 \right)^{1/2}. \quad (\text{A18})$$

For the case in which the target ends outside the brush, $h_T = h$, and Eq. (A18) is inserted into Eq. (A16) and integrated to

$$w(z) = (2B)^{1/2} \frac{h^2}{l} \left[-\frac{z}{h} \left(1 - \left(\frac{z}{h_T(z)} \right)^2 \right)^{1/2} + \cos^{-1} \left(\frac{z}{h} \right) \right] + U(h) \frac{h-z}{h} N_T \quad \text{for } z \geq h \sin \left(\frac{\pi(N_P - N_T)}{N_P} \right). \quad (\text{A19})$$

Note that Eq. (A20) reduces to Eq. (34) in Ref. 32 if $U(h) = 0$ and that $w(0) = A$, the chemical potential of a grafted chain, when $N_T = N_P$.

If the target ends within the brush, $h_T(z)$ is calculated from Eq. (A14) and Eq. (A16) is integrated to

$$w(z) = w \left[h \sin \left(\frac{\pi(N_P - N_T)}{N_P} \right) \right] + (2B)^{1/2} \frac{1}{2l^2} \left[h^2 \sin^2 \left(\frac{\pi(N_P - N_T)}{2N_P} \right) - z^2 \right] \cot \left(\frac{\pi(N_P - N_T)}{2N_P} \right) \quad \text{for } z \leq h \sin \left(\frac{\pi(N_P - N_T)}{N_P} \right). \quad (\text{A20})$$

For $z = 0$, $w(N_T) = (N_T/N_P)w(N_P)$, as predicted by Milner.

¹D. J. Graves, Trends Biotechnol. **17**, 127 (1999).

²L. M. Demers, C. A. Mirkin, R. C. Mucic, R. A. I. Reynolds, R. L. Letsinger, R. Elghanian, and G. Viswanadham, Anal. Chem. **72**, 5535 (2000).

³J. Fritz, M. K. Baller, H. P. Lang, H. Rothuizen, P. Vettiger, E. Meyer, H.-J. Guntherodt, C. Gerber, and J. K. Gimzewski, Science **288**, 316 (2000).

⁴G. Wu, H. Ji, K. Hansen, T. Thundat, R. Datar, R. Cote, M. F. Hagan, A. K. Chakraborty, and A. Majumdar, Proc. Natl. Acad. Sci. U.S.A. **98**, 1560 (2001).

⁵D. I. Stimpson, J. V. Hoijer, W. Hsieh, C. Jou, J. Gordon, T. Theriault, R. Gamble, and J. D. Baldeschwieler, Proc. Natl. Acad. Sci. U.S.A. **92**, 6379 (1994).

⁶J. J. Storhoff, R. Elghanian, R. C. Mucic, C. A. Mirkin, and R. L. Letsinger, J. Am. Chem. Soc. **120**, 1959 (1998).

⁷K. A. Peterlinz, R. M. Georgiadis, T. M. Herne, and M. J. Tarlov, J. Am. Chem. Soc. **119**, 3401 (1997).

⁸K. Hansen, H. Ji, G. Wu, R. Datar, R. Cote, A. Majumdar, and T. Thundat, Anal. Chem. **73**, 1567 (2001).

⁹A. W. Peterson, R. J. Heaton, and R. M. Georgiadis, Nucleic Acids Res. **29**, 5163 (2001).

¹⁰M. R. Henry, P. W. Stevens, J. Sun, and D. M. Kelso, Anal. Biochem. **276**, 204 (1999).

¹¹J. Zeng, A. Almadidy, J. Watterson, and U. J. Krull, Sens. Actuators A **90**, 68 (2003).

¹²Y. Okahata, M. Kawase, K. Niihara, F. Ohtake, H. Furusawa, and Y. Ebara, Anal. Chem. **70**, 1288 (1998).

¹³A. W. Peterson, R. J. Heaton, and R. M. Georgiadis, J. Am. Chem. Soc. **122**, 7837 (2000).

¹⁴A. W. Peterson, L. K. Wolf, and R. M. Georgiadis, J. Am. Chem. Soc. **124**, 14601 (2002).

¹⁵R. M. Georgiadis, K. A. Peterlinz, and A. W. Peterson, J. Am. Chem. Soc. **122**, 3166 (2000).

¹⁶V. Chan, D. J. Graves, and S. E. McKenzie, Biophys. J. **69**, 2243 (1995).

¹⁷D. Erickson, D. Li, and U. J. Krull, Anal. Biochem. **317**, 186 (2003).

¹⁸M. F. Hagan, A. Majumdar, and A. K. Chakraborty, J. Phys. Chem. B **106**, 10163 (2002).

¹⁹J. G. Wetmur and N. Davidson, J. Mol. Biol. **31**, 349 (1968).

²⁰J. G. Wetmur, Biopolymers **10**, 601 (1971).

²¹R. B. Towery, N. C. Fawcett, P. Zhang, and J. A. Evans, Biosens. Bioelectron. **16**, 1 (2002).

²²P. Schuck, Biophys. J. **70**, 1230 (1995).

²³P. Schuck and A. P. Minton, Anal. Biochem. **57**, 262 (1996).

²⁴D. R. Purvis, D. Pollard-Knight, and P. A. Lowe, in *Commercial Biosensors*, edited by G. Ramsay (Wiley-Interscience, New York, 1998), pp. 165–224.

²⁵B. Tinland, A. Pleun, J. Sturm, and G. Weill, Macromolecules **30**, 5763 (1997).

²⁶Experimental hybridization efficiencies, including recordings at later times than shown in Ref. 9, were provided by the authors.

²⁷H. H. Strey, V. A. Parsegian, and R. Podgornik, Phys. Rev. Lett. **78**, 895 (1997).

²⁸H. H. Strey, V. A. Parsegian, and R. Podgornik, Phys. Rev. E **59**, 999 (1999).

²⁹J. G. Wetmur, Crit. Rev. Biochem. Mol. Biol. **26**, 227 (1991).

³⁰The Wetmur–Davidson equation is usually written for DNA concentrations in M phosphate, in which case $k_a^B \sim Lk_N$.

- ³¹S. Misra, S. Varanasi, and P. P. Varanasi, *Macromolecules* **22**, 4173 (1989).
- ³²S. T. Milner, *Macromolecules* **25**, 5487 (1992).
- ³³N. G. van Kampen, *Stochastic Processes in Physics and Chemistry* (North-Holland, Amsterdam, 1981).
- ³⁴M. Doi and S. F. Edwards, *The Theory of Polymer Dynamics* (Oxford University Press, Oxford, 1986), Sec. 4.2.
- ³⁵D. Pörschke and M. Eigen, *J. Mol. Biol.* **62**, 361 (1971).
- ³⁶M. E. Craig, D. M. Crothers, and P. Doty, *J. Mol. Biol.* **62**, 383 (1971).
- ³⁷V. A. Bloomfield, D. M. Crothers, and I. J. Tinoco, *Nucleic Acids: Structures, Properties, and Functions* (University Science Books, Sausalito, CA, 2000).
- ³⁸A. Bar-Haim and J. Klafter, *J. Chem. Phys.* **109**, 5187 (1998).
- ³⁹P. Hänggi, P. Talkner, and M. Borkovec, *Rev. Mod. Phys.* **62**, 251 (1990).
- ⁴⁰R. Feynman, R. Leighton, and M. Sands, *The Feynman Lectures on Physics* (Addison-Wesley, Reading, MA, 1963).
- ⁴¹C. S. Peskin, G. M. Odell, and G. Oster, *Biophys. J.* **65**, 316 (1993).
- ⁴²D. T. Gillespie, *J. Phys. Chem.* **81**, 2340 (1977).
- ⁴³K. B. Froment and G. F. Bischoff, *Chemical Reactor Analysis and Design* (Wiley Series in Chemical Engineering, New York, 1979).
- ⁴⁴Due to the high charge of DNA ($2.8e$ /segment after counterion condensation) the assumption in Ref. 31 that chain ends are distributed throughout the brush is violated at low salt concentrations and high grafting densities. Consequently, the theory predicted unphysical brush heights for the results in Fig. 11 and for grafting densities higher than $\sigma=0.03$ in Fig. 7. Because the predicted rates are not sensitive to the overall brush height and there were only a few sets of experimental data to compare with, we included these results anyway.
- ⁴⁵C. G. Baumann, S. B. Smith, V. A. Bloomfield, and C. Bustamante, *Proc. Natl. Acad. Sci. U.S.A.* **94**, 6185 (1997).
- ⁴⁶S. T. Milner, T. A. Witten, and M. E. Cates, *Macromolecules* **22**, 853 (1989).
- ⁴⁷E. Giudice, P. Vrnai, and R. Lavery, *Phys. Chem. Chem. Phys.* **2**, 673 (2001).
- ⁴⁸E. Giudice, P. Vrnai, and R. Lavery, *Nucleic Acids Res.* **31**, 1434 (2003).
- ⁴⁹N. K. Banavali and A. D. J. MacKerell, *J. Mol. Biol.* **319**, 141 (2002).
- ⁵⁰N. Huang, N. K. Banavali, and A. D. J. MacKerell, *Proc. Natl. Acad. Sci. U.S.A.* **100**, 68 (2003).
- ⁵¹M. F. Hagan, A. R. Dinner, D. Chandler, and A. K. Chakraborty, *Proc. Natl. Acad. Sci. U.S.A.* **100**, 13922 (2003).
- ⁵²S. T. Milner, T. A. Witten, and M. E. Cates, *Macromolecules* **21**, 2610 (1988).
- ⁵³G. J. Fleer, M. A. Cohen Stuart, J. M. H. M. Scheutjens, T. Cosgrove, and B. Vincent, *Polymers at Interfaces* (Chapman and Hall, London, 1993).
- ⁵⁴P. G. De Gennes, *Macromolecules* **13**, 1069 (1980).
- ⁵⁵A. N. Semenov, *Zh. Eksp. Teor. Fiz.* **88**, 1242 (1985).
- ⁵⁶G. S. Manning, *J. Chem. Phys.* **51**, 924 (1969).
- ⁵⁷G. S. Manning, *J. Chem. Phys.* **51**, 3249 (1969).
- ⁵⁸F. Oosawa, *Polyelectrolytes* (Marcel Dekker, New York, 1971).
- ⁵⁹M. Muthukumar, *J. Chem. Phys.* **105**, 5183 (1996).
- ⁶⁰C. N. Patra and A. Yethiraj, *J. Phys. Chem. B* **103**, 6080 (1999).